C. R. Physique 13 (2012) 426–439

Contents lists available at SciVerse ScienceDirect

Comptes Rendus Physique

www.sciencedirect.com

Advances in nano-electromechanical systems

Mechano-electronic and electro-mechanical energy transfer in mesoscopic superconducting weak links

Transfert d'énergie mécano-électronique et électromécanique dans des connexions mésoscopiques supraconductrices faibles

Robert I. Shekhter [a,*], Leonid Y. Gorelik [b], Gustav Sonne [a], Mats Jonson [a,c,d]

[a] *Department of Physics, University of Gothenburg, SE-412 96 Göteborg, Sweden*
[b] *Department of Applied Physics, Chalmers University of Technology, SE-412 96 Göteborg, Sweden*
[c] *SUPA, Department of Physics, Heriot–Watt University, Edinburgh EH14 4AS, Scotland, UK*
[d] *Department of Physics, Division of Quantum Phases and Devices, Konkuk University, Seoul 143-107, Republic of Korea*

ARTICLE INFO

Article history:
Available online 30 March 2012

Keywords:
Nano-electro-mechanical systems
Superconducting weak links

Mots-clés :
Systèmes nano-électromécaniques
Connexions supraconductrices faibles

ABSTRACT

In this review we discuss how the nano-electro-mechanical properties of a superconducting weak link, formed by a suspended nanowire bridging two superconductors, can strongly affect mesoscopic effects in both the electronic and the mechanical subsystem. In particular we will discuss how quantum coherence and electron–electron (Coulomb) correlations may result in the possibility to resonantly redistribute energy between the electronic and mechanical degrees of freedom, allowing controllable switching between pumping and cooling of the nano-mechanical vibrations of the suspended nanowire. The two regimes of a given current and a given voltage supplied to the nano-electro-mechanical weak link is considered, resulting respectively in the possibility of ground-state cooling or resonant generation of nano-mechanical vibrations for realistic experimental parameters.

RÉSUMÉ

Dans cet article nous décrivons comment les propriétés nano-électromécaniques d'une connexion faible formée par un nanofil suspendu entre deux supreconducteurs, peut fortement affecter les effets mésoscopiques dans le sous-système électronique comme dans le sous-système. Nous décrirons en particulier comment la cohérence quantique et les corrélations de Coulomb entre électrons peuvent rendre possible une redistribution résonante de l'énergie entre les degrés de liberté électroniques et mécaniques, permettant d'alterner de façon contrôlée le pompage et le refroidissement des vibrations nano-mécaniques du nanofil. On considère deux régimes dans lesquels on fixe soit le courant, soit la tension agissant sur la connexion nano-électromécanique, le résultat étant respectivement un refroidissement dans l'état fondamental ou la génération résonante de vibrations nano-mécaniques, obtenus pour des paramètres expérimentaux réaliste.

* Corresponding author.
E-mail address: robert.shekhter@physics.gu.se (R.I. Shekhter).

1631-0705/$ – see front matter
doi:10.1016/j.crhy.2012.01.002

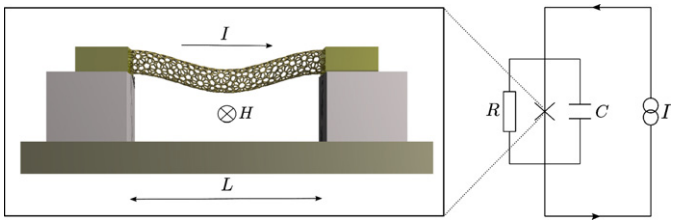

Fig. 1. Schematic diagram of the system under consideration. (Left) A suspended nanowire of length L forms a weak link between two current-biased superconducting leads. The transverse magnetic field H is applied perpendicular to the nanowire. (Right) The equivalent electronic circuit. A constant current I is applied to the Josephson junction which is connected in parallel to a capacitor C and a resistance R.

1. Introduction

In this review we will discuss how the coupling between conduction electrons and mechanical bending modes in nano-electro-mechanical systems (NEMS) may provide not only signal transduction between electrical and mechanical degrees of freedom but also cause energy to be transferred between the two subsystems. In principle, energy may flow in either direction over a sustained period of time, which means that the nano-mechanical subsystem can be either heated or cooled, depending on the mode of operation of the device. We will describe heating as the result of an "electro-mechanical" energy flow (to the mechanical subsystem) and associate cooling with a "mechano-electronic" energy flow (from the mechanical subsystem). The question of the direction of the energy flow and how to control it externally is one of the most important issues in modern NEMS research, not only for fundamental research but also for practical applications. While the pumping of energy transferred from the electronic degrees of freedom into the mechanical subsystem provides the most conventional form of actuation in electro-mechanical devices to date, see e.g. Refs. [1–13], the electronic cooling of nano-mechanical systems is of central importance in the current discussion of quantum manipulation of mechanical degrees of freedom [14–24].

By reducing the size of the electro-mechanical devices one decreases the number of degrees of freedom available to the system, thereby restricting the applicability of conventional macroscopic thermodynamics for describing the energy flow through such devices. The eventual failure of the macroscopic approach is due to the increasing role of fluctuations in systems with fewer and fewer degrees of freedom. Two regimes can be distinguished; one is the microscopic regime, where the degrees of freedom really are very few and hence fluctuations are important, and the other is the mesoscopic regime where in spite of the fact that the number of degrees of freedom is not small, fluctuations in observable quantities are nevertheless large. While the microscopic regime is now coming under discussion [25], the regime of mesoscopic energy transfer can readily be reached in sub-micron samples. We will show that in this case two prominent mesoscopic effects – quantum coherence and Coulomb blockade of tunnelling – qualitatively affect the energetics of nano-electro-mechanical devices. In doing so, we will consider a particular type of nano-electro-mechanical device, where a suspended nanowire is allowed to carry an electrical current in the presence of an external magnetic field, see Fig. 1. The electromotive coupling induced by the magnetic field serves to couple the flexural vibrations of the nanowire to the electrical current flowing through it. Below, we analyse how this coupling may modify the mechano-electronic and electro-mechanical energy transfer when the electronic leads connecting the system are superconducting. The motivation behind the choice to study superconducting devices is that these systems are the best candidates for observing both macroscopic quantum coherence and Coulomb blockade phenomena, making them ideal candidates for detection and manipulation of the mechanical vibrations at or close to the quantum limit, see e.g. Refs. [26–32].

The outline of this article is as follows. In Section 2 we introduce the reader to the concept of nano-electro-mechanics in Josephson weak links. In Section 3 we analyse how the electro-mechanical coupling induced by the magnetic field may result in pumping of the suspended nanowire vibrations, thereby transferring energy from the electronic to the mechanical degrees of freedom in a voltage-biased junction. By instead current-biasing the junction we show in Section 4 that the same coupling can be used to transfer energy in the opposite direction, thereby cooling the vibrations of the suspended nanowire to close to the quantum limit. Finally we summarise our findings in Section 5.

2. Mesoscopic nano-electro-mechanics of Josephson weak links

A Josephson weak link that is short on the scale of the superconducting coherence length $\xi = \hbar v_F/\Delta_0$, where v_F is the Fermi velocity and Δ_0 is the superconducting gap, can be thought of as an interface between two superconductors and phenomenologically characterised by a transmission probability D. A nonzero transmission probability implies a coupling between the two superconductors, which in the limit $D \ll 1$ forms a weak superconducting link. The quantum coherence of the electronic Andreev states, which form at the interface and are responsible for this coupling (see Ref. [33] and references therein), gives rise to a strongly nonlinear dependence of the electrical current through the weak link on ϕ, that is on the phase difference between the superconducting condensates on either side of the interface. This nonlinear dependence is of course manifested in the dc and ac Josephson effects. Coulomb correlation effects, caused by accumulation of charge at the interface as a result of electronic back-scattering, may make it necessary to treat ϕ as an operator $\hat{\phi}$ with quantum

dynamics, rather than as a c-number. Both the quantum dynamics of the superconducting phase difference ϕ and the nonlinear dependence of the current through the Josephson weak link on ϕ appear for small enough weak links (either in a direction parallel to or perpendicular to the current) and should be considered as mesoscopic properties of the device.

The Andreev states, which appear at the interface between the two superconductors due to the Josephson coupling between them, can be viewed as the degree of freedom of the device responsible for the supercurrent flow. The device is sketched in Fig. 1, where the phenomenologically introduced capacitance C and resistance R characterise the electrostatic response of the device to the electric charge accumulation and the dissipation due to quasi-particle excitations, respectively.

The quantum dynamics of the Josephson weak link can be described through the following Hamiltonian [34],

$$\hat{H} = 4E_c\hat{n}^2 - E_J\cos\hat{\phi} \tag{1}$$

Here, the $\hat{n} = \partial/\partial\hat{\phi}$ is the canonical conjugate operator to the superconducting phase operator $\hat{\phi}$ and represents the electrical charge transferred between the superconductors due to the tunnelling of Cooper pairs [35]. In (1), $E_c = e^2/(2C)$ is the Coulomb energy and E_J is the Josephson energy with e the electronic charge.

Zero point oscillations of the superconducting phase defined in the Hamiltonian (1) are of order $\delta\phi \sim E_c/E_J$. In the limit of negligible Coulomb effects, $E_c \ll E_J$, quantum fluctuations of the superconducting phase disappear, and the classical dynamics of the superconducting weak link is recovered. For the case when the junction is biased by a voltage V, it follows that

$$I = I_c\sin\phi \tag{2a}$$

$$\frac{\partial\phi}{\partial t} = \frac{2eV}{\hbar} \tag{2b}$$

Here, I is the current through the device and $I_c = (2e/\hbar)E_J$ is the critical current. Eqs. (2) imply that in the limit of weak Coulomb effects, the current through the device is dictated by the phase difference according to Eq. (2a).

For the case when Coulomb correlations cannot be neglected, the quantum dynamics of the weak link is governed by the Hamiltonian (1). In this case, the ground state wave function is localised to the minima of the Josephson potential, which occur for $\phi = 2n\pi$, $n = 0, 1, 2, 3\ldots$. By expanding the potential in the vicinity of these minima, weakly excited electronic states are obtained corresponding to a spectrum of electronic states separated by the Josephson plasma oscillation frequency ω_p,

$$E_k = (k+1/2)\hbar\omega_p = (k+1/2)\sqrt{8E_cE_J}, \quad k = 0, 1, 2, 3, \ldots \tag{3}$$

In this case, the current through the system is given as the quantum average of the derivative of the Hamiltonian with respect to the operator $\hat{\phi}$. To account for this under conditions when the device is biased by a constant current I one may modify the Hamiltonian (1) to include the Lagrange multiplier $-j\hbar\hat{\phi}$ where $j = I/(2e)$,

$$\hat{H} = 4E_c\hat{n}^2 - j\hbar\hat{\phi} - E_J\cos\hat{\phi} \tag{4}$$

For the devices considered here, mechanical degrees of freedom are introduced through the flexural vibrations of the suspended nanowire [36–39].[1] The electronic degrees of freedom are affected by the inclusion of the mechanical element either through a shift of the electronic energy levels or as a change in the electronic tunnelling probability due to displacements of the nanowire. If these two mechanisms of electro-mechanical coupling appear simultaneously, an electro-mechanical shuttle instability may occur due to the transfer of electronic charge through the device [1]. Additional possibilities for nano-electro-mechanical operation occurs if the movable element is part of a superconducting weak link. In this case, time dependent dynamics of the system may occur even at dc driving of the system. As a result, resonant electro-mechanical coupling can be achieved even if only one of the two coupling mechanisms mentioned above is present. In this review we will focus on the specifics of these mechanisms for the case of superconducting weak link junctions.

The physics of electro-mechanical coupling considered here can be based either on displacement dependent charge accumulation at the weak link or on electromotive coupling to the electronic current flowing through the device. In the first case, a so-called polaronic coupling occurs through the time dependent electrostatic force on the wire due to variation (in time) of electronic charge injection into weak link. In a second case, which is only possible when an external magnetic field is applied, a Lorenz force (and complementary to it an electromotive force) are responsible for the mutual influence of mechanical and electronic degrees of freedom. These electromotive coupling mechanisms will here be considered as examples of nano-electro-mechanical phenomena. Here we neglect the removal of the spin-degeneracy of electronic energy levels by the magnetic field, considering the energy shift $2mu_BH$ (μ_B is the Bohr magneton) to be small on the scale of the relevant energies E_J and E_c. However, under different circumstances this energy shift can be responsible for nonlinear effects in the transport of spin-polarised electrons in magnetic devices [41].

[1] Systems where the mechanical degrees of freedom are introduced as a displacement of the centre of mass of the weak link with respect to the bulk leads or a gate electrode were discussed in Ref. [40].

The flexural vibrations of the suspended nanowire that forms the weak link may be described by expanding the motion of the nanowire in its normal modes. Under such considerations, the mechanical displacement of the nanowire can be formulated as a set of harmonic oscillations expressing the dynamics of the amplitude of oscillation as a function of time. By considering resonant coupling of electrons to such modes (as well as a significant difference in frequency between different modes) we may restrict our analysis to consider the effects of the electro-mechanical coupling with only a single vibrational mode which we here take to be the lowest flexural mode whose eigenfrequency we denote by ω.[2] Depending on the level of description of the evolution of the mechanical degrees of freedom, we may considered either a classical Newtonian or quantum mechanical description for the displacement of the nanowire. In a first case the equation of motion of the flexural vibrations of the nanowire is given by,

$$m\ddot{u} + \gamma\dot{u} + m\omega^2 u = F_{el} \tag{5}$$

In (5), u is the displacement of the central part of the wire in the direction perpendicular to its longitudinal axis, γ is a phenomenological damping coefficient introduced to account for dissipation in the mechanical subsystem, m is the mass of the nanowire and F_{el} is the force acting on the nanowire due to the electro-mechanical coupling. If instead the quantum description applies, the dynamics of mechanical displacement is determined by the harmonic-oscillator Hamiltonian

$$\hat{H}_{mech} = \hbar\omega\big(\hat{b}^\dagger\hat{b} + 1/2\big) \tag{6}$$

where $\hat{b}$ [$\hat{b}^\dagger$] are operators which annihilate [create] one quantum of mechanical vibration. For the case of a quantum description, any effect of damping (either of the mechanical or electronic subsystem) has to be included phenomenologically in the evolution of the associated density matrix (see Section 4).

In the absence of quantum fluctuations, the classical description of the mechanical degrees of freedom is sufficient to describe the system (see Section 3). In this case, we find that energy may be pumped into the mechanical system, resulting in a large amplitude of mechanical displacement at resonant driving. If these fluctuations may not be neglected, a full quantum analysis is needed (Section 4) in which case we find that we may also use the electronic subsystem to cool the mechanical vibrations of the nanowire to close to the quantum ground state.

Finally, the effects of the mechanical displacement on the electronic subsystem should be addressed. As will be discussed further below, these effects may be included into the analysis of the electro-mechanical system through a renormalisation of the evolution of the superconducting phase in the Josephson term of the electronic energy. Such a renormalisation takes into account the additional voltage drop (electromotive force) caused by the mechanical motion of the current carrying conductor in the presence of an external magnetic field (see Ref. [45]),

$$\phi \to \phi - \frac{4eLHu}{\hbar} \tag{7}$$

The problem of the coupled electro-mechanical dynamics in nano-electro-mechanical weak links formulated above will be considered in the following sections. There we will focus on the effects of quantum coherence and Coulomb correlations and how these determine the observable phenomena due to the electro-mechanical coupling. In the next section (Section 3), the effects of Coulomb blockade will be neglected, a restriction which is valid as long as the Josephson coupling is the dominant mechanism. In Section 4 we relax this restriction to consider also the effects of Coulomb correlations on the electro-mechanics of the device.

3. Superconductive pumping of nano-mechanical vibrations

In the first instance we will consider the possibility to transform electronic energy to mechanical energy in a voltage-biased nano-electro-mechanical junction as was originally analysed in Ref. [45], see Fig. 1. The junction considered is taken to have low transparency to electrons tunnelling between the leads such that a Josephson-type description of the electronic degrees of freedom is applicable. Through the use of a transverse magnetic field we show that the alternating supercurrent over the junction, provided by the applied battery, couples to the mechanical degrees of freedom through the induced Lorentz force. Below we analyse the outcome of this coupling and show that pronounced vibrational motion of the suspended nanowire can be achieved at resonant conditions. These vibrations are associated with an energy transfer from the battery to the vibrations of the nanowire, where the mechanical damping γ dictates the efficiency of this energy transfer.[3]

In the low transparency limit, $D \ll 1$, the bound Andreev states which describe the electronic degrees of freedom in the system are widely separated in energy and the current through the wire is to a good approximation given by the Josephson relation (2). For the parameters considered, $I_c = D\Delta_0 e/(2\hbar) \sim 100$ nA is the critical current where $\Delta_0 \sim 10$ meV. In what follows, we perform a classical evaluation of the pumped vibrations for the case of a nanowire of length $L \sim 1$ μm in a magnetic field $H \sim 20$ mT.

[2] Coupling to the higher modes may also be considered, see e.g. Refs. [42–44].

[3] The inductive coupling between flexural wire vibrations and the supercurrent flow in a SQUID loop has been considered in Refs. [46,47,31,32].

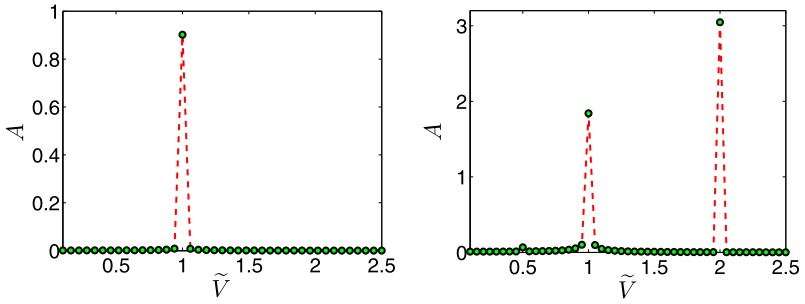

Fig. 2. Numerical simulation of Eq. (8) for the time-averaged vibrational amplitude $A = \sqrt{\langle Y(t)^2 \rangle}$ as a function of the bias voltage $\tilde{V}$ for two different driving strengths ϵ.

The Josephson relation implies that the current I through the wire will oscillate in time as the phase difference changes due to the applied bias voltage V. The transverse magnetic field now serves two purposes. First, it will induce a force on the wire due to the current through it, the Lorentz force, which is proportional to the product $I_c LH$. Secondly, the motion of the wire in the magnetic field will induce an electromotive force which tries to oppose the motion causing it.[4] In Ref. [45] we show that the expression for the electromotive force can be formally derived from the Bogoliubov–de Gennes equation which describes the electronic degrees of freedom of the superconducting junction (see also Ref. [48] for further details of this derivation). The outcome of this analysis is that the phase difference over the junction depends on the motion of the nanowire in the magnetic field $\dot{\phi}(t) \propto V - LH\dot{u}(t)$ where $u(t)$ is the vibrational amplitude of the nanowire and the dots indicate the time derivative. Alternatively this can be seen as the back-action on the electronic system from the motion of the nanowire in the magnetic field.

The magnetic field thus determines both the force on the wire due to the flow of charge carriers through it and the evolution of the phase difference due the motion of the wire. Formally this is described by the dimensionless equations of motion (see Eq. (5)) for the deflection coordinate $Y(t) = u(t)4eLH/\hbar$ and phase $\phi(t)$,

$$\ddot{Y} + \tilde{\gamma}\dot{Y} + Y = \epsilon \sin(\phi) \tag{8a}$$

$$\dot{\phi} = \tilde{V} - \dot{Y} \tag{8b}$$

where time is measured in units of $1/\omega$. In (8), $\tilde{\gamma} = 1/Q$ is the damping coefficient of the nanowire where Q is the mechanical quality factor, $Q \sim 1000$. The electro-mechanical coupling is here given by $\epsilon = 8e^2H^2L^2I_c/(m\hbar\omega^2)$ which gives the driving strength on the nanowire. Finally, $\tilde{V} = 2eV/(\hbar\omega)$ is the dimensionless bias voltage. Following Ref. [45] we consider the suspended nanowire in the form of a carbon nanotube for which the lowest vibrational mode is $\omega \sim 1$ GHz.

The dynamics of the vibrating nanowire is governed by Eqs. (8). Performing detailed numerical and analytical analysis we find that the effect of the electro-mechanical coupling is that the vibrations of the nanowire can be pumped to finite amplitude under resonant conditions as depicted in Fig. 2. Furthermore, we find that this pumping not only occurs at the resonance frequency $\tilde{V} = 1$ but also that the parametric resonance $\tilde{V} = 2$ can be excited at higher driving force as displayed in Fig. 2(b).[5] In Ref. [45] it is shown that this behaviour is well explained through the two stability equations,

$$\dot{X}_n = -\tilde{\gamma}X_n - 2\epsilon n J_n(\sqrt{X_n}) \sin\chi_n \tag{9a}$$

$$\dot{\chi}_n = -\delta - 2\epsilon n J_n'(\sqrt{X_n}) \cos\chi_n \tag{9b}$$

where the amplitude X_n and phase χ_n are slow functions of time at resonance (see Appendix A for a derivation of the stability equations). In (9), J_n are Bessel functions of order $n = 1, 2, \ldots$ with J_n' being the derivative with respect to X_n and $\delta = \tilde{V} - n$ measures the voltage offset from resonance.

The system considered will perform stable motion (vibrations with constant amplitude) if neither the amplitude X_n nor phase χ_n change in time, i.e. both equations (9) are simultaneously 0. At resonance, $\delta = 0$, this is found either at fixed phase $\cos\chi_n = 0$ or fixed amplitude $J_n'(\sqrt{X_n}) = 0$. For the parametric resonance $\tilde{V} = 2$ such motion is only found once the driving force is $\epsilon \geqslant \epsilon_I = 2\tilde{\gamma}$, whereas the first resonance peak is always present at finite driving. Also, the vibrational amplitude is initially an increasing function of the driving force (for both peaks), which eventually saturates to finite vibrations once the driving force is $\epsilon \geqslant \epsilon_{II} = \tilde{\gamma}X_n^*/(2nJ_n(\sqrt{X_n^*}))$ where X_n^* corresponds to the fixed amplitude solution $J_n'(\sqrt{X_n^*}) = 0$ as shown in Fig. 3(a).[6]

[4] This is Lenz's law; the induced current (or in this case phase) is always in a direction which is opposite to the change causing it.

[5] Also higher resonance modes, i.e. $\tilde{V} = 3, 4, \ldots$ can be found. However, by choosing the nanowire to be initially at rest these solutions cannot be reached as their region of stability is separated from the origin by a separatrix.

[6] The notation X_n^* and $A_n^* = \sqrt{X_n^*}$ is used interchangeably throughout this section. In Ref. [45] these are referred to as A_0.

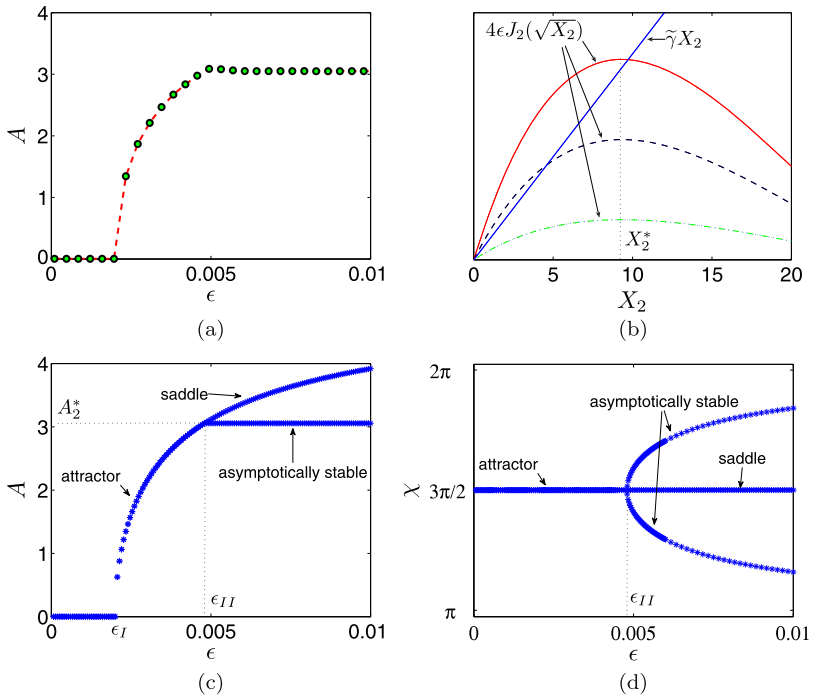

Fig. 3. (a) Numerical simulation of the vibrational amplitude, Eq. (8), at the second resonance as a function of the driving strength. (b) Plot of the solution $\dot{X}_2 = 0$ in (9) for $\chi_2 = 3\pi/2$ for three different driving strengths, $\epsilon < \epsilon_I$ (dot-dashed (green) line), $\epsilon_I < \epsilon < \epsilon_{II}$ (dashed (black) line) and $\epsilon > \epsilon_{II}$ (solid (red) line). (c)–(d) Corresponding stability diagram for the amplitude and phase as a function of the driving strength.

These phenomena are explained through the solution of (9). At $\delta = 0$ there always exists a solution $X_n = 0$ (no periodic vibrations of the wire). The stability of this solution is found by considering the expansion of the Bessel functions for small arguments X, $J_n(\sqrt{X}) \sim X^{n/2}$. With this one finds that the solution $X_n = 0$ is always unstable for $n = 1$ and becomes unstable for $n = 2$ at $\epsilon > \epsilon_I = 2\tilde{\gamma}$. Thus, the peak at $\tilde{V} = 1$ is always present for nonzero driving, whereas the peak at $\tilde{V} = 2$ is only found once $\epsilon > \epsilon_I$ as shown in Figs. 3(a) and 3(c). At larger driving strengths $\epsilon > \epsilon_I$, the amplitude is an increasing function of ϵ (fixed phase solution) corresponding to the crossing of the two curves in Fig. 3(b). However, once the driving is large enough that this crossing moves past X_n^*, the fixed phase stability point becomes a saddle point and the system follows the trajectory of the fixed amplitude solution. This is shown in Figs. 3(c) and 3(d), from which we infer that the nanowire vibrates at the finite amplitude A_n^* for all $\epsilon > \epsilon_{II}$ if driven at resonance. A final check of the validity of the stability analysis is to analyse the numerical solutions for the different resonance peaks (different n) at $\delta = 0$ over the type-I regimes. From (9) we expect the ratio $X_n/(n\epsilon J_n(\sqrt{X_n}))$ to be constant for all peaks at a given $\tilde{\gamma}$ in this regime. Comparing this with the numerical simulations we find excellent agreement.

Moving off resonance, $|\delta| \neq 0$, one finds the width of the peaks by solving for δ in Eqs. (9),

$$\left(\frac{\tilde{\gamma}X_n}{2\epsilon n J_n(\sqrt{X_n})}\right)^2 + \left(\frac{\delta}{2\epsilon n J_n'(\sqrt{X_n})}\right)^2 = 1 \tag{10}$$

For the parametric resonance $n = 2$ this implies that the total width of the peak is $2|\delta| = 2(\epsilon^2/4 - \tilde{\gamma}^2)^{1/2}$. Furthermore, Eq. (10) has two stable solutions for the vibrational amplitude within the interval $(-\delta_c, \delta_c)$ at $\epsilon > \epsilon_{II}$. These solutions correspond to a separation of the fixed amplitude solutions in phase space with one solution being larger and the other smaller than the fixed amplitude solution X_n^* at small $|\delta|$. This is shown in Fig. 4(b) for the second resonance peak. As $|\delta|$ is increased the solution which is larger than I_n^* merges with the saddle point (defined by the fixed phase solution) at $|\delta_c|$ and only one stable point (corresponding to the low amplitude solution) remains at larger $|\delta|$. Close to the transition to the fixed amplitude solution, $\epsilon = \epsilon_{II} + \Delta\epsilon$ with $\Delta\epsilon \ll \epsilon_{II}$, the width of the window of bistability $2\delta_c$ scales as $(\Delta\epsilon)^{3/2}$ as discussed in Appendix A.

The pumping of the mechanical vibrations draws energy from the battery connecting the junction. This implies a finite dc current I_{dc} through the junction. At resonance this current provides the energy necessary to compensate for the mechanical dissipation associated with $\tilde{\gamma}$,

$$I_{dc} = \frac{\tilde{\gamma}\langle\dot{Y}^2\rangle m\hbar\omega^2}{8eL^2H^2\tilde{V}} = \frac{\gamma\langle\dot{u}^2(t)\rangle}{V} \tag{11}$$

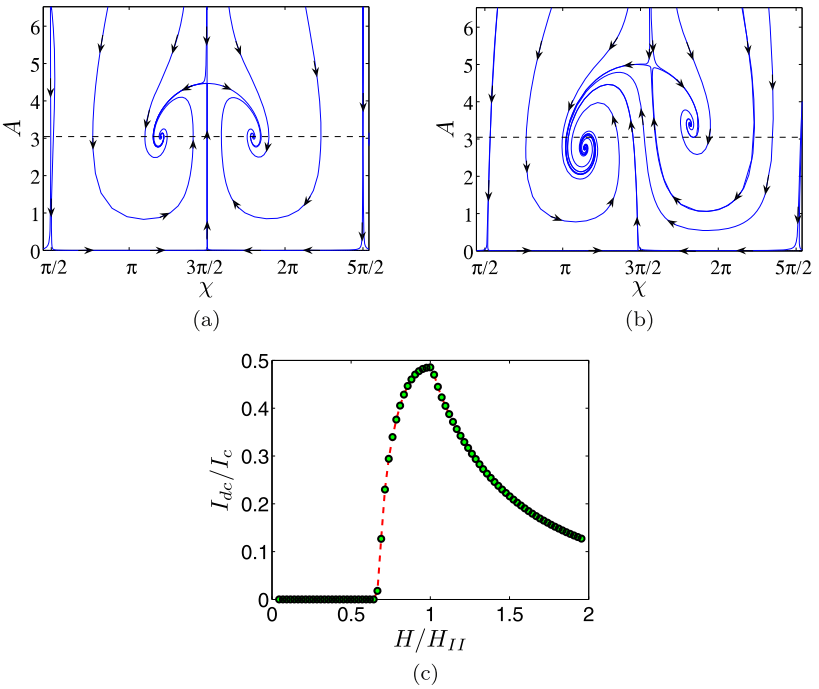

Fig. 4. Phase space diagram for the second resonance peak at $\epsilon > \epsilon_{II}$. In (a) $\delta = 0$, two solutions can be found at the same amplitude. In (b) $0 < \delta < \delta_c$, the solutions are separate in phase space. The dashed line corresponds to the fixed amplitude solution. (c) Current through the system at $\delta = 0$ at the parametric resonance as a function of the magnetic field. Here, H_{II} is the magnetic field corresponding to ϵ_{II}.

Physically this implies that the current scales with the time-average velocity squared (see Appendix A for details on the derivation of the dc current). As the velocity $\dot{Y}$ and amplitude Y of the mechanical motion of the wire behave phenomenologically equivalent at resonance this implies that the system originally analysed in Ref. [45] displays both positive and negative differential magnetoresistance. To see this, consider at first the system when driven at resonance $\delta = 0$ in the regime $\epsilon_I < \epsilon < \epsilon_{II}$. In this range, the amplitude is an increasing function of the magnetic field and the current correspondingly increases with H (negative magnetoresistance). However, once $\epsilon > \epsilon_{II}$ the vibrational amplitude saturates, and the current scales as H^{-2} under which conditions the system displays positive magnetoresistance. The transition between these two regimes is experimentally observable as a cusp as seen in Fig. 4(c). The observable dc current through over the junction has been estimated to $I_{dc} \sim 50$ nA which corresponds to a vibrational amplitude of the mid-point of the nanowire of ~ 25 nm.

4. Cooling of a voltage-biased vibrating superconducting weak link

Next we turn our attention to the possibility to transfer energy from the mechanical to the electronic subsystem, thereby cooling the motion of the suspended nanowire resonator. The analysis presented below was originally published in Ref. [49] and considers a similar experimental setup as in the section above, however we now consider the junction to be biased by a constant current rather than a constant voltage.[7] In this section we thus consider the possibility to cool (rather than heat) the mechanical vibrations of the nanowire through the absorption of mechanical vibrons by the electronic subsystem. In order to do so, we perform a full quantum calculation of the system where the electronic degrees of freedom are described through the so-called RCSJ-model and analyse the possibility to cool the vibrations of the nanowire through a phenomenon known as macroscopic quantum tunnelling.

In the RCSJ-model, the current-biased Josephson junction is modelled as a circuit element connected in parallel to a capacitance C and a resistance R as shown in Fig. 1. As we discussed in Section 2, in this kind of junction the time-evolution of the phase difference ϕ is described through an equation which is equivalent to that of a particle moving in a tilted cosine potential. This potential is usually referred to as the tilted washboard potential (see e.g. Ref. [52]) an example of which is shown in Fig. 5 where the tilting angle is proportional to the bias current I and the height and width of the valleys is determined from the physical parameters of the Josephson junction.

By changing the bias current the tilt of the washboard potential can be altered. In particular this implies that the phase ϕ can be highly localised to one of the minima of the potential if $\hbar I/(2e) < E_J$. The equation for the phase in any one of

[7] In the case of a voltage-biased junction the mechanical subsystem can also be cooled to close to the quantum limit, see Refs. [50,51].

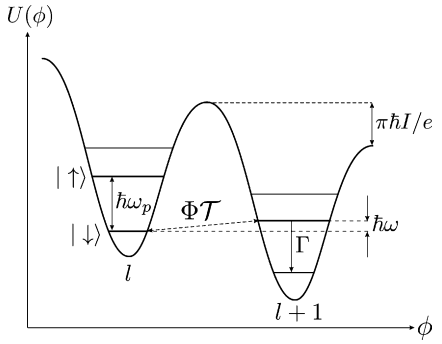

Fig. 5. Schematic diagram of the tilted washboard potential $U(\phi) = -E_J \cos\phi - j\hbar\phi$ as a function of phase ϕ at current-bias $I = e/\pi(\omega_p - \omega)$. Here, l labels the valleys of the potential and $\sigma = \uparrow, \downarrow$ are the two energy levels within the valleys considered. In the above, $\Phi\mathcal{T}$ is the inelastic tunnelling amplitude between two energy levels in consecutive valleys. The quantity Γ is the transition rate from the second to the first level within a valley generated by interactions with the quasi-particle environment (see text).

the valleys of the tilted washboard potential is phenomenologically equivalent to that of a particle trapped in a virtually parabolic well. Under such conditions, one expects quantised energy levels for the phase inside the valleys of the potential as indicated in Fig. 5 (see Ref. [34] for a more detailed discussion). Experimentally, this prediction has been confirmed in association with tunnelling of the quantum phase from bound energy states between consecutive valleys of the washboard potential, a phenomenon which is known as macroscopic quantum tunnelling (MQT), see e.g. Refs. [53–55]. This kind of under-barrier tunnelling is the underlying cooling mechanism considered in this analysis.

In Ref. [49] we analyse how the coupling between the electronic degrees of freedom and the oscillating nanowire affects the dynamics of the system. The magnetic field is here considered to provide the electro-mechanical coupling in a similar way as in the previous section. This implies that we treat the motion of the short (compared to the superconducting coherence length) nanowire in the magnetic field as resulting in a modulation of the evolution of the phase difference, $\phi \to \phi - 4eLHu/\hbar$ where all the symbols have the same meaning as in the previous sections. Under such considerations the quantum Hamiltonian describing the system is given by Eq. (12), a derivation of which is given in Appendix B starting from the analysis of Ref. [45],

$$\hat{\mathcal{H}} = 4E_c\hat{n}^2 - j\hbar\hat{\phi} - E_J\cos(\hat{\phi} - \Phi\hat{u}) + \hbar\omega\hat{b}^\dagger\hat{b} \tag{12}$$

In (12) the conjugate quantum variables $\hat{n}$ and $\hat{\phi}$ describe respectively the electronic charge and phase over the junction ($[\hat{\phi}, \hat{n}] = i$). The operator $\hat{u} = \hat{b} + \hat{b}^\dagger$ is the deflection of the nanowire which is here treated as a quantum oscillator where $\hat{b}$ [$\hat{b}^\dagger$] annihilate [create] a vibrational quantum. Here, $\Phi = 4g\pi LHu_{zp}/\Phi_0$ is the electro-mechanical coupling constant where g is a geometric factor of order unity, u_{zp} is the zero point amplitude of the nanowire oscillator and $\Phi_0 = \pi\hbar/e$.

The conditions outlined above implies the inter-level spacing between the two lowest energy levels within a given valley of the washboard potential, $\hbar\omega_p = (8E_JE_c)^{1/2}$, is much smaller than the height of the barrier separating the different valleys, see Fig. 5. Under such conditions, the quantum phase is trapped in the minima of the potential, however it may tunnel under the barrier separating two consecutive valleys, thereby resulting in a potential drop over the junction, $\dot{\phi} \propto V$. Such macroscopic quantum tunnelling events are greatly promoted if the two energy levels involved in the process are resonant, which can be controlled by the external bias current. With this, we define the critical current I^* as the current which ensures that the lowest (first) level is resonant with the second level in the next valley, $I^* \simeq e\omega_p/\pi$ [34]. This condition also implies that we may neglect all but the two lowest energy levels as the overlap between the higher energy levels will be small if the energy separation between the two lowest levels is of the order of $\hbar\omega$ (for experimental parameters $\omega \ll \omega_p$).

The electro-mechanical coupling induced by the magnetic field implies that MQT can in the present situation also be accompanied by emission/absorption of a quantum of mechanical energy.[8] To analyse the effect of this coupling we perform a WKB calculation (see Ref. [34] for reference) for the overlap integrals for both the elastic (no interaction with the mechanical subsystem) and inelastic (absorption/emission of a mechanical vibron by the electronic subsystem) tunnelling channels. From this analysis we find that the inelastic tunnelling channels $\propto \Phi(\hat{b} + \hat{b}^\dagger)$ are proportional to the elastic tunnelling amplitude $\mathcal{T} \propto \hbar\omega_p \exp(-\pi(E_J/(2E_c))^{1/2})$ under conditions of strong quantisation, $4E_c/E_J \ll 1$. With this, we may express the inelastic tunnelling amplitudes as $\Phi\mathcal{T}$, where the inelastic absorption [emission] channel is associated with the absorption [emission] of one quantum of energy $\hbar\omega$ from the mechanical to the electronic subsystem. This is shown in Fig. 5 where the absorption channel is assumed to be in resonance $I = I^* - e\omega/\pi$, i.e. the two bound energy states are separated by one quantum of mechanical energy $\hbar\omega$. Note that due to the large separation in energy $\omega \ll \omega_p$, the electro-mechanical coupling will not introduce additional tunnelling channels between the higher levels.

[8] Here, we consider only the linear expansion of the Hamiltonian (12) in the coupling parameter $\Phi < 1$.

Tunnelling through the inelastic channels changes the number of mechanical vibrons in the system. Below we show that this may result in cooling (heating) of the mechanical subsystem if the absorption (emission) channel is resonant. A further condition to ensure that the cooling processes discussed here will lower the effective temperature of the nanowire oscillator is that the electronic subsystem, once in the second energy level, relaxes to the lower level in the same valley at a rate Γ which is faster than the rate at which the system tunnels back with the emission of a vibron, $\Gamma > \mathcal{T}/\hbar$. Such relaxation of the electronic subsystem arises from interactions with the quasi-particle environment in the superconducting leads. In Ref. [49] these effects are included in the analysis through the phenomenological resistance R, see Fig. 1 with $\Gamma = 1/(RC)$ the electronic decay rate [56]. Furthermore, interactions with the quasi-particle environment lead to broadening of the energy levels of the order of $\Delta\omega_p = \omega_p/(2Q_{el})$. For the system considered it is reasonable to assume $Q_{el} \gg 1$, which implies that the influence from the electronic quasi-particle environment on the tunnelling processes is negligible [34,56, 57].

To perform a quantitative analysis of the system we introduce the basis $|l,\sigma\rangle$ where $\sigma = \uparrow, \downarrow$ labels the energy levels inside a given valley ($\downarrow$ is the first and $\uparrow$ is the second level) and l labels the valleys of the tilted washboard potential. In this basis the Hamiltonian (12) reads,

$$\hat{\mathcal{H}} = \hat{\mathcal{H}}_0 + \hat{\mathcal{H}}_{\mathcal{T}}$$
$$\hat{\mathcal{H}}_0 = \sum_{l,n,\sigma} \big(\mathcal{F}_{l,\sigma} + \hbar\omega \hat{b}^\dagger \hat{b}\big)|l,\sigma\rangle\langle l,\sigma|, \qquad \hat{\mathcal{H}}_{\mathcal{T}} = \sum_l \mathcal{T}\big(\Phi\big(\hat{b} + \hat{b}^\dagger\big) + 1\big)|l+1,\uparrow\rangle\langle l,\downarrow| + \text{h.c.} \tag{13}$$

In the above, $\mathcal{F}_{l,\sigma} = \hbar\omega_p m_\sigma - l\pi\hbar I/e$ are the eigenvalues for the electronic degrees of freedom in the basis $|l,\sigma\rangle$, where $m_\uparrow = 1$ and $m_\downarrow = 0$. It is clear from the above that the number of mechanical vibrons in the system can change through macroscopic quantum tunnelling of the electronic system from one valley to the next. The joint dynamics of the electronic and mechanical degrees of freedom is described through the Liouville–von Neumann equation for the density matrix $\hat{\rho}$ of the system,

$$\frac{\partial\hat{\rho}}{\partial t} = -\frac{i}{\hbar}[\hat{\mathcal{H}}_0 + \hat{\mathcal{H}}_{\mathcal{T}}, \hat{\rho}] + \hat{J}(\hat{\rho}) + \gamma(1+n_B)\mathcal{L}_{\hat{b}}(\hat{\rho}) + \gamma n_B \mathcal{L}_{\hat{b}^\dagger}(\hat{\rho}) \tag{14}$$

Here, $\hat{J}(\hat{\rho})$ is a phenomenological damping operator for the electronic system,

$$\hat{J}(\hat{\rho}) = -\frac{\Gamma}{2}\sum_l \big\{\hat{\rho}|l,\uparrow\rangle\langle l,\uparrow| + |l,\uparrow\rangle\langle l,\uparrow|\hat{\rho}\big\} + \Gamma\sum_{l,l'} |l,\downarrow\rangle\langle l,\uparrow|\hat{\rho}|l',\uparrow\rangle\langle l',\downarrow| \tag{15}$$

which derives from the resistance R as discussed above [34]. In (14), the operator $\mathcal{L}_{\hat{a}}(\hat{\rho}) = (2\hat{a}\hat{\rho}\hat{a}^\dagger - \hat{a}^\dagger\hat{a}\hat{\rho} - \hat{\rho}\hat{a}^\dagger\hat{a})/2$, is the standard Lindblad operator which models interactions between the oscillator and the thermal environment. Here, $\gamma = \omega/Q$ is the mechanical damping rate and $n_B = (\exp(\beta\hbar\omega) - 1)^{-1}$, where $\beta = (k_B T)^{-1}$, is the average number of vibrons in thermal equilibrium.

Below we investigate the stationary solution to (14). To find this solution we perform a standard perturbative analysis in the small parameters $\mathcal{T}/(\hbar\Gamma)$, $\gamma/\Gamma \propto \epsilon \ll 1$ and look for a solution of the density matrix of the form $\hat{\rho} = \hat{\rho}_0 + \epsilon\hat{\rho}_1 + \epsilon^2\hat{\rho}_2 + \cdots$ (see Appendix B for a full derivation of the results presented below). Substituting this into (14) one finds that the leading order solution $\hat{\rho}_0$ has the form $\hat{\rho}_0 = \sum_{l,n} |l,\downarrow,n\rangle\rho_0(l,\downarrow,n)\langle l,\downarrow,n|$, where the index n labels the Fock state of the oscillator. From (14) we also calculate the first order correction to the density matrix $\hat{\rho}_1 = \sum_{l,n,j=-1,0,1} |l+1,\uparrow,n+j\rangle c_j(l,n)\langle l,\downarrow,n| +$ h.c. With this, the equation for the second order term, $\hat{\rho}_2$, can only be resolved if the coefficients $P(n) = \sum_l \rho_0(l,\downarrow,n)$ – which give the population of the vibrational modes of the oscillator – satisfy the following equation,

$$\big(\Gamma_- + \gamma(1+n_B)\big)\big[(n+1)P(n+1) - nP(n)\big] + (\Gamma_+ + \gamma n_B)\big[nP(n-1) - (n+1)P(n)\big] = 0 \tag{16}$$

Here, Γ_j are the tunnelling rates; $j = -, 0, +$ is respectively the absorption, elastic and emission channel,

$$\Gamma_\pm = \Gamma\frac{4\Phi^2\mathcal{T}^2}{4(\Delta\mathcal{F}_\pm)^2 + \hbar^2\Gamma^2}, \qquad \Gamma_0 = \Gamma\frac{4\mathcal{T}^2}{4(\Delta\mathcal{F}_0)^2 + \hbar^2\Gamma^2}$$
$$\Delta\mathcal{F}_0 = \mathcal{F}_{l+1,\uparrow} - \mathcal{F}_{l,\downarrow}, \qquad \Delta\mathcal{F}_\pm = \Delta\mathcal{F}_0 \pm \hbar\omega$$

Tunnelling of the phase introduces a potential drop over the Josephson junction as discussed above. To analyse this we introduce the operator for the potential drop $\hat{V} = i[\hat{\mathcal{H}}, \hat{\phi}]/(2e)$ (in our representation $\hat{\phi} = 2\pi\sum_{l,\sigma} |l,\sigma\rangle l\langle l,\sigma|$),

$$\hat{V} = \frac{\pi}{ie}\sum_l \mathcal{T}\big(\Phi\big(\hat{b} + \hat{b}^\dagger\big) + 1\big)|l+1,\uparrow\rangle\langle l,\downarrow| + \text{h.c.} \tag{17}$$

This implies that the bias voltage, $V = \text{Tr}(\hat{V}\hat{\rho})$, is zero (the phase is stationary) to leading order in $\hat{\rho}$, and that the potential drop is given by the first order correction to the density matrix, $V = \text{Tr}(\hat{V}\hat{\rho}_1)$. Solving Eq. (16) one finds that the results for the coefficients $P(n)$ correspond to a thermal distribution of vibron excitations characterised by an effective temperature,

$$T_{\text{eff}} = \frac{\hbar\omega}{k_B}\left[\ln\left(\frac{\Gamma_- + \gamma(1+n_B)}{\Gamma_+ + \gamma n_B}\right)\right]^{-1} \tag{18}$$

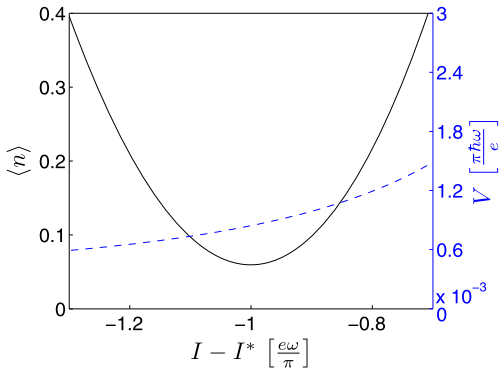

Fig. 6. Average vibron population (solid) and bias voltage (dashed) in the stationary regime as a function of the current bias. Here, $\Phi = 0.3$, $\Gamma = \omega/4$, $\mathcal{T} = \hbar\omega/20$, $n_B = 20$ and $Q = 10^5$.

which is different from the ambient temperature T except in the limit $\gamma \gg \Gamma_\pm$. Furthermore, the analytical solution for the average number of vibrons, $\langle n\rangle = \sum_n nP(n)$ and the bias voltage V are given by

$$\langle n\rangle = \frac{n_B\gamma + \Gamma_+}{\gamma + \Gamma_- - \Gamma_+} \tag{19}$$

$$V = \frac{\pi\hbar}{e}\big(\Gamma_-\langle n\rangle + \Gamma_0 + \Gamma_+\big(\langle n\rangle + 1\big)\big) \tag{20}$$

Note that he potential drop in the stationary regime scales with the elastic tunnelling rate, Γ_0 and the average vibron occupancy. This is consistent with the physical processes discussed, i.e. in the limit $\gamma, \Gamma_+ \to 0$ we get $\langle n\rangle = 0$ (complete ground state cooling as no heating channel is open) and $V \propto \Gamma_0$ (the system moves down the potential at the rate Γ_0 which conserves the number of vibrons). Note, however, that Γ_0 does not enter into the analytic solution of $\langle n\rangle$. This can be understood as MQT through the elastic channel does not change the number of vibrons in the system.

In Fig. 6 we plot both the average stationary population of the mechanical subsystem and the corresponding voltage drop as a function of the bias current. As expected, the lowest occupation is achieved when $I = I^* - e\omega/\pi$ (see Fig. 5). In this regime, we find that ground state cooling of the mechanical subsystem is possible if the resolved side-band limit, $\omega > \Gamma$, is achieved. Under conditions when the bias current is $I > I^*$ the tunnelling events discussed above will lead to pumping of the mechanical subsystem, in which case the above analysis does not apply once the limit $\mathcal{T}(\langle n\rangle + 1) \sim \hbar\Gamma$ is reached.

5. Conclusion

We have shown that mesoscopic phenomena can prominently affect the superconducting electro-mechanics on the nanometre length scale. In particular, we have described how quantum coherence and Coulomb correlations can control the redistribution of energy supplied to the NEM device from an external voltage or current source, resulting in a tunable switching between pumping or cooling of the nano-mechanical vibrations. Both these effects, i.e. mechano-electronic and electro-mechanical energy transformation, can be detected electronically through observations of current spikes in the voltage-biased setup and voltage spikes in the current-biased mode of operation. For both setups we have considered realistic experimental parameters and find that pronounced mesoscopic phenomena is expected in the electro-mechanical operation of the device. As an example, the level of cooling achievable for the current-biased geometry is sufficient to maintain the nanowire close to its ground state.

In this review we have considered only the limit of strong electronic back-scattering, when only a single Andreev level is involved in the NEM dynamics. In the opposite limit of a nearly ballistic superconducting weak link, the Andreev level spacing can be significantly reduced. In this case, inter-Andreev level transitions assisted by the absorption/emission of a vibrational quantum also become possible [58,59], a phenomenon which is observable as a reversal of the direction of supercurrent flow. As was shown in Refs. [50] and [51], a nano-electro-mechanical weak link can in this mode of operation work as a refrigerator for the mechanical vibrations where the voltage-driven Andreev levels absorb energy from the mechanical subsystem and transfer it to a quasi-particle thermostat in the superconducting leads. This phenomenon opens additional possibilities for ground-state cooling of the nano-mechanical vibrations similarly to what has been discussed in this review.

Acknowledgements

This work was supported in part by the Swedish VR and SSF, by the EC project QNEMS (FP7-ICT-233952) and by the Korean WCU program (MEST/KOSEF R31-2008-000-10057-0).

Appendix A. Derivation and analysis of the stability equations

A.1. Stability equations

Starting from Eq. (8), the stability equations (9) can be found by introducing the ansatz $Y(t) = \sqrt{X_n(t)}\sin(\Theta(t))$ where $\Theta(t) = \tilde{V}t/n + \chi_n(t)/n$. Close to resonance both the amplitude X_n and phase χ_n are slow functions of time. Substituting the expression for $Y(t)$ into (8) we find two equations which govern X_n and χ_n when $\tilde{V} \simeq n$. Integrating these over the period Θ, we arrive at the stability equations of the system (9),

$$\dot{X}_n = -\tilde{\gamma} X_n + 2n\frac{\partial \mathcal{H}_{\text{eff}}}{\partial \chi_n}, \qquad \dot{\chi}_n = n - \tilde{V} - 2n\frac{\partial \mathcal{H}_{\text{eff}}}{\partial X_n}$$

$$\mathcal{H}_{\text{eff}} = \frac{\epsilon}{2\pi}\int_{-\pi}^{\pi} \cos\bigl(n\Theta - \chi_n - \sqrt{X_n}\sin(\Theta)\bigr)\,\mathrm{d}\Theta$$

$$\mathcal{H}_{\text{eff}} = \epsilon\, J_n(\sqrt{X_n})\cos(\chi_n) \tag{A.1}$$

A.2. Scaling of the bifurcation amplitude with the magnetic field

To find the scaling of the bifurcation amplitude with the magnetic field we expand the solutions of (9) close to the transition from the constant phase to the constant amplitude solution, i.e. we consider $\epsilon = \epsilon_{II} + \Delta\epsilon$ with $\Delta\epsilon \ll \epsilon_{II}$. At $\epsilon = \epsilon_{II}$ the stable solution is given by $J_n(\sqrt{X_n^*}) = 0$ and $\chi_n^* = (2n-1)\pi/2$. Expanding the solution about this point we find,

$$-\tilde{\gamma}\,\Delta X_n + 2n\Delta\epsilon\, J_n\bigl(\sqrt{X_n^*}\bigr) = \frac{J_n(\sqrt{X_n^*})\delta^2}{4n\epsilon_{II}|J_n''(\sqrt{X_n^*})|^2(\Delta X_n)^2} \tag{A.2}$$

where $\Delta X_n = X_n - X_n^*$. Note that in the above $\tilde{\gamma}$ is uniquely defined by ϵ_{II} through $\tilde{\gamma} = 2\epsilon_{II} n J_n(\sqrt{X_n^*})/X_n^*$. From Eq. (A.2) we calculate the maximum separation in the vibrational amplitude which is found from the zeros of the cubic equation,

$$\left(\Delta X_n - \frac{2\alpha}{3}\right)^2\left(-\Delta X_n - \frac{\alpha}{3}\right) = 0, \quad \alpha = \frac{2n\Delta\epsilon\, J_n(\sqrt{X_n^*})}{\tilde{\gamma}} \tag{A.3}$$

With this, the maximum separation in amplitude between the two solutions scale as $X_n^*\Delta\epsilon/\epsilon_{II}$. Furthermore, it can be shown that,

$$\frac{\delta^2 J_n(\sqrt{X_n^*})}{4n\epsilon_{II}|J_n''(\sqrt{X_n^*})|^2\tilde{\gamma}} = \frac{1}{2}\left(\frac{2\alpha}{3}\right)^3 \tag{A.4}$$

which implies that we can solve for δ,

$$\delta = (\Delta\epsilon)^{3/2}\left(\frac{2X_n^*}{3\epsilon_{II}}\right)^{3/2}\left(\frac{2n\epsilon_{II}|J_n''(\sqrt{X_n^*})|^2}{X_n^*}\right)^{1/3} \tag{A.5}$$

to find that the width of the window of bistability scales with the magnetic field as H^3 close to the region of bifurcation.

A.3. dc current

The dc current through the system is calculated by considering the energy dissipation due to the damping of the mechanical vibrations. This can be shown by multiplying (8) throughout by $\dot{Y}$ and averaging over time. At resonance, the total energy associated with the harmonic oscillator $E \propto \dot{Y}^2 + Y^2$ does not change in time. This implies that the total energy dissipated by the mechanical system $\tilde{\gamma}\langle\dot{Y}^2\rangle$ is related to the current drawn from the battery according to,

$$\tilde{\gamma}\bigl\langle\dot{Y}^2\bigr\rangle = \frac{\epsilon}{T}\int_{-T/2}^{T/2} \dot{Y}\sin(\tilde{V}\tau - Y)\,\mathrm{d}\tau, \quad \tau = \omega t \tag{A.6}$$

Evaluating the right-hand side of (A.6) we eliminate the dependence of $\dot{Y}$ and find,

$$\tilde{\gamma}\bigl\langle\dot{Y}^2\bigr\rangle = \epsilon\tilde{V}\frac{I_{dc}}{I_c} \tag{A.7}$$

The corresponding expression for the dc current I_{dc} is,

$$I_{dc} = \frac{\tilde{\gamma}\langle\dot{Y}^2\rangle m\hbar\omega^2}{8eL^2H^2\tilde{V}} = \frac{\gamma\langle\dot{u}^2(t)\rangle}{V} \tag{A.8}$$

Appendix B. Derivation of system Hamiltonian and the stationary solution of the density matrix

B.1. System Hamiltonian

The Hamiltonian (12) can be derived starting from the classical equations of motion of the system. Referring to Fig. 1 these can be expressed as,

$$\frac{\partial\phi}{\partial t} = \frac{2eq}{\hbar C} - \frac{4eLH}{\hbar}\dot{u} \tag{B.1a}$$

$$\frac{\partial q}{\partial t} = I - \frac{2eE_J}{\hbar}\sin\phi \tag{B.1b}$$

$$m\ddot{u} = -ku + 2LH\left(\frac{2eE_J}{\hbar}\sin\phi\right) \tag{B.1c}$$

In the above, q is the charge on the capacitor C such that the bias voltage over the junction is $V = q/C$. In (B.1a), the evolution of the phase difference ϕ depends on the motion of the nanowire in the magnetic field ($\dot{u}$ is the velocity of the nanowire) which follows from the analysis of Section 3 and Ref. [45]. Eq. (B.1b) gives the time rate of charge on the capacitor (note that the resistance R is not included here as it is introduced as a damping term in the evolution of the density matrix). Finally, Eq. (B.1c) gives the equation of motion of the nanowire subject to the periodic driving force due to the alternating Josephson current over the junction. The corresponding system Hamiltonian reads,

$$\mathbb{H} = 4E_c n^2 - \frac{4eLH}{m}p_u n + \frac{8e^2L^2H^2}{m}n^2 + \frac{p_u^2}{2m} + \frac{ku^2}{2} - 4eLHj_0u - j\hbar\phi - E_J\cos\phi \tag{B.2}$$

where $n = q/(2e)$ is the number of Cooper pairs, $j = I/(2e)$ is the Cooper pair current and p_u is the momentum of the nanowire. Quantisation is achieved by regarding the variables a, p_a, ϕ and n as Hermitian operators satisfying the following commutation relations $[\hat{u}, \hat{p}_u]/\hbar = [\hat{\phi}, \hat{n}] = i$ and $[\hat{u}, \hat{\phi}] = [\hat{u}, \hat{n}] = [\hat{p}_u, \hat{\phi}] = [\hat{p}_u, \hat{n}] = 0$. With this we perform the unitary transformation,

$$\hat{\mathcal{H}} = e^{-i\Phi\hat{u}\hat{n}}\hat{\mathbb{H}}e^{i\Phi\hat{u}\hat{n}}, \quad \Phi = \frac{4\pi gLHu_{zp}}{\Phi_0} \tag{B.3}$$

after which the Hamiltonian reads,

$$\hat{\mathcal{H}} = 4E_c\hat{n}^2 - j\hbar\hat{\phi} - E_J\cos\left(\hat{\phi} - \Phi\left(\hat{b} + \hat{b}^\dagger\right)\right) + \hbar\omega\hat{b}^\dagger\hat{b} \tag{B.4}$$

Here we use the notation $\hat{u} = \hat{b} + \hat{b}^\dagger$ for the deflection operator with $u_{zp} = [\hbar/(2m\omega)]^{1/2}$ the zero point amplitude of the oscillating nanowire.

B.2. Stationary solution of the density matrix

The evolution of the density matrix is governed by the Liouville–von Neumann equation (14),

$$\frac{\partial\hat{\rho}}{\partial t} = -\frac{i}{\hbar}[\hat{\mathcal{H}}_0 + \hat{\mathcal{H}}_{\mathcal{T}}, \hat{\rho}] + \hat{J}(\hat{\rho}) + \gamma(1+n_B)\mathcal{L}_{\hat{b}}(\hat{\rho}) + \gamma n_B\mathcal{L}_{\hat{b}^\dagger}(\hat{\rho}) \tag{B.5}$$

In what follows we will consider the stationary solution of (B.5) by performing a perturbative analysis in the small parameters $\mathcal{T}/(\hbar\Gamma), \gamma/\Gamma \ll 1$. In particular we will consider the limit of high mechanical quality factor Q such that $\gamma = \omega/Q < \mathcal{T}/(\hbar)$. To start the analysis we take the total density matrix to be of the form, $\hat{\rho} = \hat{\rho}_0 + \epsilon\hat{\rho}_1 + \epsilon^2\hat{\rho}_2 + \cdots$ and equate powers of ϵ. With this we find the following equations,

$$0 = -\frac{i}{\hbar}[\hat{\mathcal{H}}_0, \hat{\rho}_0] + \hat{J}(\hat{\rho}_0) \qquad O\left(\epsilon^0\right) \tag{B.6a}$$

$$0 = -\frac{i}{\hbar}[\hat{\mathcal{H}}_0, \hat{\rho}_1] + \hat{J}(\hat{\rho}_1) - \frac{i}{\hbar}[\hat{\mathcal{H}}_{\mathcal{T}}, \hat{\rho}_0] \qquad O\left(\epsilon^1\right) \tag{B.6b}$$

$$0 = -\frac{i}{\hbar}[\hat{\mathcal{H}}_0, \hat{\rho}_2] + \hat{J}(\hat{\rho}_2) - \frac{i}{\hbar}[\hat{\mathcal{H}}_{\mathcal{T}}, \hat{\rho}_1] + \gamma(1+n_B)\mathcal{L}_{\hat{b}}(\hat{\rho}_0) + \gamma n_B\mathcal{L}_{\hat{b}^\dagger}(\hat{\rho}_0) \qquad O\left(\epsilon^2\right) \tag{B.6c}$$

Solving the above equations at each order of ϵ we find $\hat{\rho}_0 = \sum_{l,n}|l,\downarrow,n\rangle\rho_0(l,\downarrow,n)\langle l,\downarrow,n|$ which satisfies (B.6a). Similarly, the first order correction to the stationary density matrix is determined from (B.6b) as,

$$\hat{\rho}_1 = \sum_{l,n,\,j=-1,0,1}|l+1,\uparrow,n+i\rangle c_j(l,n)\langle l,\downarrow,n| + \text{h.c.} \tag{B.7a}$$

$$c_j(l,n) = \frac{\mathcal{T}_j^{(n)}\rho_0(l,\downarrow,n)}{-\Delta\mathcal{F}_j + i\hbar\Gamma/2} \tag{B.7b}$$

Substituting this into (B.6c) we find the equation for the coefficients ρ_0 by tracing out the spin $(\uparrow,\downarrow)$ degrees of freedom,

$$\begin{aligned}&\Gamma\sum_{j=-1,0,1}\frac{4}{4(\Delta\mathcal{F}_j)^2+\hbar^2\Gamma^2}\big(\big|\mathcal{T}_j^{(n-j)}\big|^2\rho_0(l-1,\downarrow,n-j)-\big|\mathcal{T}_j^{(n)}\big|^2\rho_0(l,\downarrow,n)\big)\\&=\gamma(1+n_B)\big[n\rho_0(l,\downarrow,n)-(n+1)\rho_0(l,\downarrow,n+1)\big]+\gamma n_B\big[(n+1)\rho_0(l,\downarrow,n)-n\rho_0(l,\downarrow,n-1)\big]\end{aligned}\tag{B.8}$$

Tracing out the valley index l we recover the expressions presented in Section 4, i.e. Eq. (B.7b) gives

$$C_j(n)\equiv\sum_{l=-\infty}^{\infty}c_j(l,n)=\frac{\mathcal{T}_j^{(n)}P(n)}{-\Delta\mathcal{F}_j+i\hbar\Gamma/2}$$

whereas Eq. (B.8) gives,

$$\big(\Gamma_-+\gamma(1+n_B)\big)\big[(n+1)P(n+1)-nP(n)\big]+(\Gamma_++\gamma n_B)\big[nP(n-1)-(n+1)P(n)\big]=0\tag{B.9}$$

In this expression the relationship between the coefficients are,

$$\Gamma_\pm=\Gamma\frac{4\Phi^2\mathcal{T}^2}{4(\Delta\mathcal{F}_\pm)^2+\hbar^2\Gamma^2},\qquad\Gamma_0=\Gamma\frac{4\mathcal{T}^2}{4(\Delta\mathcal{F}_0)^2+\hbar^2\Gamma^2}$$

$$\frac{i}{\hbar}\mathcal{T}_j^{(n)}\big(C_j(n)-C_j^*(n)\big)=P(n)\Gamma_jN,\quad N=\begin{cases}n+1 & j=+\\ 1 & j=0\\ n & j=-\end{cases}$$

In the above we note that (B.9) gives the balanced equation for the probability $P(n)$ of finding the oscillating nanowire in the state n. By regrouping the terms in this equation one can write it on the form

$$(n+1)\big[C_-P(n+1)-C_+P(n)\big]-n\big[C_-P(n)-C_+P(n-1)\big]=0\tag{B.10}$$

where

$$C_-=\Gamma_-+\gamma(1+n_B)\quad\text{and}\quad C_+=\Gamma_++\gamma n_B\tag{B.11}$$

This is convenient, since it is clear that a solution to (B.10), and hence to (B.9), requires that the relation

$$\frac{P(n+1)}{P(n)}=\frac{C_+}{C_-}\tag{B.12}$$

holds for all n. This means that $P(n)$ describes a thermal distribution of vibron excitations characterised by an effective temperature implicitly defined by the relation $P(n+1)/P(n)=\exp(-\hbar\omega/k_BT_{\text{eff}})$. Using (B.11) and (B.12) one finds the explicit result

$$T_{\text{eff}}=\frac{\hbar\omega}{k_B}\left[\ln\left(\frac{\Gamma_-+\gamma(1+n_B)}{\Gamma_++\gamma n_B}\right)\right]^{-1}$$

The stationary average distribution of the vibrational modes is obtained from (B.10)–(B.12) as

$$\langle n\rangle=\sum_{n=0}^{\infty}nP(n)=\frac{n_B\gamma+\Gamma_+}{\Gamma_-+\gamma-\Gamma_+}$$

The density matrix $\hat{\rho}_1$ allows us to evaluate the potential drop over the junction in the stationary regime. Following the derivation outlined above we find that the lowest order term of the density matrix, $\hat{\rho}_0$, does not contribute to the potential drop as it is diagonal in the spin basis. As such, the potential drop is uniquely determined from $\hat{\rho}_1$.

References

[1] L.Y. Gorelik, A. Isacsson, M.V. Voinova, B. Kasemo, R.I. Shekhter, M. Jonson, Phys. Rev. Lett. 80 (1998) 4526.
[2] A. Isacsson, L.Y. Gorelik, M.V. Voinova, B. Kasemo, R.I. Shekhter, M. Jonson, Physica B 255 (1998) 150.
[3] D. Fedorets, L.Y. Gorelik, R.I. Shekhter, M. Jonson, Europhys. Lett. 58 (2002) 99.
[4] H. Park, J. Park, A.K.L. Lim, E.H. Anderson, A.P. Alivisatos, P.L. McEuen, Nature 407 (2000) 57.
[5] L.Y. Gorelik, A. Isacsson, Y.M. Galperin, R.I. Shekhter, M. Jonson, Nature 411 (2001) 454.
[6] A. Erbe, C. Weiss, W. Zwerger, R.H. Blick, Phys. Rev. Lett. 87 (2001) 096106.
[7] D. Fedorets, Phys. Rev. B 68 (2003) 033106.
[8] T. Novotny, A. Donarini, A.-P. Jauho, Phys. Rev. Lett. 90 (2003) 256801.
[9] D.V. Scheible, R.H. Blick, Appl. Phys. Lett. 84 (2004) 4632.
[10] D. Fedorets, L.Y. Gorelik, R.I. Shekhter, M. Jonson, Phys. Rev. Lett. 92 (2004) 166801.
[11] L.M. Jonsson, L.Y. Gorelik, R.I. Shekhter, M. Jonson, Nano Lett. 5 (2005) 1165.

[12] R.I. Shekhter, L.Y. Gorelik, M. Jonson, Y.M. Galperin, V.M. Vinokur, J. Comput. Theor. Nanosci. 4 (2007) 860.
[13] A.V. Moskalenko, S.N. Gordeev, O.F. Koentjoro, P.R. Raithby, R.W. French, F. Marken, S.E. Savel'ev, Phys. Rev. B 79 (2009) 241403.
[14] M.P. Blencowe, Contemp. Phys. 46 (2005) 249.
[15] M.L. Roukes, Phys. World 14 (2001) 25.
[16] I. Wilson-Rae, P. Zoller, A. Imamoğlu, Phys. Rev. Lett. 92 (2004) 075507.
[17] I. Martin, A. Shnirman, L. Tian, P. Zoller, Phys. Rev. B 69 (2004) 125339.
[18] K.C. Schwab, M.L. Roukes, Phys. Today 58 (2005) 36.
[19] M.L. Roukes, in: Technical Digest of the 2000 Solid-State Sensor and Actuator Workshop, Cleveland, 2000.
[20] S.H. Ouyang, J.Q. You, F. Nori, Phys. Rev. B 79 (2009) 075304.
[21] F. Pistolesi, J. Low Temp. Phys. 154 (2009) 199.
[22] S. Zippilli, G. Morigi, A. Bachtold, Phys. Rev. Lett. 102 (2009) 096804.
[23] S. Zippilli, A. Bachtold, G. Morigi, Phys. Rev. B 81 (2010) 205408.
[24] J.D. Teufel, T. Donner, D.L. Li, J.W. Harlow, M.S. Allman, K. Cicak, A.J. Sirois, J.D. Whittaker, K.W. Lehner, R.W. Simmonds, Nature 475 (2011) 359.
[25] N. Linden, S. Popescu, P. Skrzypczyk, Phys. Rev. Lett. 105 (2010) 130401.
[26] A. Naik, O. Buu, M.D. LaHaye, A.D. Armour, A.A. Clerk, M.P. Blencowe, K.C. Schwab, Nature 443 (2006) 193.
[27] M.D. LaHaye, O. Buu, B. Camarota, K.C. Schwab, Science 304 (2004) 74.
[28] R.G. Knobel, A.N. Cleland, Nature 424 (2003) 291.
[29] T. Rocheleau, T. Ndukum, C. Macklin, J.B. Hertzberg, A.A. Clerk, K.C. Schwab, Nature 463 (2010) 72.
[30] A.D. O'Connell, M. Hofheinz, M. Ansmann, R.C. Bialczak, M. Lenander, E. Lucero, M. Neely, D. Sank, H. Wang, M. Weides, et al., Nature 464 (2010) 697.
[31] S. Etaki, M. Poot, I. Mahboob, K. Onomitsu, H. Yamaguchi, H.S.J. van der Zant, Nat. Phys. 4 (2008) 785.
[32] M. Poot, S. Etaki, I. Mahboob, K. Onomitsu, H. Yamaguchi, Y.M. Blanter, H.S.J. van der Zant, Phys. Rev. Lett. 105 (2010) 207203.
[33] C.W.J. Beenakker, Phys. Rev. Lett. 67 (1991) 3836.
[34] J.M. Schmidt, A.N. Cleland, J. Clarke, Phys. Rev. B 43 (1991) 229.
[35] K.K. Likharev, A.B. Zorin, J. Low Temp. Phys. 59 (1985) 347.
[36] V. Sazonova, Y. Yaish, H. Üstünel, D. Roundy, T.A. Arias, P.L. McEuen, Nature 431 (2004) 284.
[37] D. Garcia-Sanchez, A.S. Paulo, M.J. Esplandiu, F. Perez-Murano, L. Forró, A. Aguasca, A. Bachtold, Phys. Rev. Lett. 99 (2007) 085501.
[38] A.K. Hüttel, M. Poot, B. Witkamp, H.S.J. van der Zant, New J. Phys. 10 (2008) 095003.
[39] A.K. Hüttel, G.A. Steele, B. Witkamp, M. Poot, L.P. Kouwenhoven, H.S.J. van der Zant, Nano Lett. 9 (2009) 2547.
[40] R.I. Shekhter, Y. Galperin, L.Y. Gorelik, A. Isacsson, M. Jonson, J. Phys.: Condens. Matter 15 (2003) R441.
[41] L.Y. Gorelik, S.I. Kulinich, R.I. Shekhter, M. Jonson, V.M. Vinokur, Phys. Rev. Lett. 95 (2005) 116806.
[42] L.M. Jonsson, L.Y. Gorelik, R.I. Shekhter, M. Jonson, New J. Phys. 9 (2007) 90.
[43] L.M. Jonsson, F. Santandrea, L.Y. Gorelik, M. Jonson, Phys. Rev. Lett. 100 (2008) 186802.
[44] F. Santandrea, Phys. Res. Int. (2010) 493478.
[45] G. Sonne, R.I. Shekhter, L.Y. Gorelik, S.I. Kulinich, M. Jonson, Phys. Rev. B 78 (2008) 144501.
[46] E. Buks, M.P. Blencowe, Phys. Rev. B 74 (2006) 174504.
[47] E. Buks, E. Segev, S. Zaitsev, B. Abdo, M.P. Blencowe, Europhys. Lett. 81 (2008) 10001.
[48] R.I. Shekhter, F. Santandrea, G. Sonne, L.Y. Gorelik, M. Jonson, J. Low Temp. Phys. 35 (2009) 662.
[49] G. Sonne, L.Y. Gorelik, Phys. Rev. Lett. 106 (2011) 167205.
[50] G. Sonne, M.E. Peña-Aza, L.Y. Gorelik, R.I. Shekhter, M. Jonson, Phys. Rev. Lett. 104 (2010) 226802.
[51] G. Sonne, M.E. Peña-Aza, L.Y. Gorelik, R.I. Shekhter, M. Jonson, J. Low Temp. Phys. 36 (2010) 902.
[52] M. Tinkham, Introduction to Superconductivity, 2nd ed., Dover Publications, Mineola, 1996.
[53] J.M. Martinis, M.H. Devoret, J. Clarke, Phys. Rev. Lett. 55 (1985) 1543.
[54] S. Han, Y. Yu, X. Chu, S.-I. Chu, Z. Wang, Science 293 (2001) 1457.
[55] Y. Yu, S. Han, X. Chu, S.I. Chu, Z. Wang, Science 296 (2002) 889.
[56] D. Esteve, M.H. Devoret, J.M. Martinis, Phys. Rev. B 34 (1986) 158.
[57] N. Hatakenaka, H. Takayanagi, S. Kurihara, Physica B 165–166 (1990) 931.
[58] L.Y. Gorelik, V.S. Shumeiko, R.I. Shekhter, G. Wendin, M. Jonson, Phys. Rev. Lett. 75 (1995) 1162.
[59] L.Y. Gorelik, N.I. Lundin, V.S. Shumeiko, R.I. Shekhter, M. Jonson, Phys. Rev. Lett. 81 (1998) 2538.